DOI: 10.17725/rensit.2022.14.197

Holographic Processing of Moving Sources in a Shallow Sea with Intense Internal Waves

Venedikt M. Kuz'kin
Prokhorov Institute of General Physics of RAS, http://www.gpi.ru/
Moscow 119991, Russian Federation
E-mail: kumiov@yandex.ru

Sergey A. Pereselkov, Elena S. Kaznacheeva, Sergey A. Tkachenko, Pavel V. Rybyanets
Voronezh State University, http://www.vsu.ru/
Voronezh 394006, Russian Federation
E-mail: pereselkov@yandex.ru, elna.kaznacheeva@yandex.ru, sega-th@mail.ru, rybyanets.edu@yandex.ru

Vladimir I. Grachev
Kotelnikov Institute of Radioengineering and Electronics of RAS, http://www.cplire.ru/
Moscow 125009, Russian Federation
E-mail: grachev@cplire.ru

Received May 4, 2022; peer-reviewed May 11, 2022; accepted May 18, 2022

Abstract: **In a shallow water area for two frequency ranges, on the basis of numerical simulation, the influence of intense internal waves that cause the interaction of sound field modes on the formation of an interferogram and a hologram of a moving source is considered. On the hologram, the spectral densities of the source field corresponding to the unperturbed and perturbed waveguides are separated. This made it possible to reconstruct the interferogram of the unperturbed field in the presence of intense internal waves. The relative error of its reconstruction is determined. The effect of a disturbance on the reconstruction of the distance and radial velocity of a source in the presence of a disturbance is estimated.**

Keywords: **shallow sea, interferogram, hologram, intense internal waves, mode interaction, moving sound source**

UDC 004.052.34

Acknowledgments: This work was supported by the Russian Foundation for Basic Research (project no. 19-29-06075). The work of E.S. Kaznacheeva was supported by a grant from the President of the Russian Federation MK-6144.2021.4. The work of S.A. Tkachenko was supported by a grant from the President of the Russian Federation MK-4846.2022.4.

For citation: Venedikt M. Kuz'kin, Sergey A. Pereselkov, Elena S. Kaznacheeva, Vladimir I. Grachev, Sergey A. Tkachenko, Pavel V. Rybyanets. Holographic Processing of Moving Sources in a Shallow Sea with Intense Internal Waves. *RENSIT: Radioelectronics. Nanosystems. Information Technologies,* 2022, 14(2):197-204e. DOI: 10.17725/rensit.2022.14.197.

Contents

1. INTRODUCTION

The problem of detection and localization of low-noise underwater sources is one of the poorly developed problems in ocean acoustics. Difficulties in the approach to its solution stem from the limitations of the

applied mathematical models for describing the source signal. Currently, active interest from many scientific teams is attracted by the solution of the problem based on holographic processing based on stable structural features of the interference pattern of the sound field formed by a broadband sound source. We note the main works [1−4], where significant results were obtained in this direction for regular waveguides.

Holographic processing implements quasi-coherent accumulation of spectral density along localized fringes of an interference pattern (interferogram) in frequency-time variables. An interferogram is understood as the square of the module of the received signal in frequency-time variables. The location geometry of the localized bands is determined by the parameters of the waveguide, the speed and trajectory of the sound source. A two-dimensional Fourier transform (2D-FT) is applied to the accumulated spectral density of the interferogram. At the output of the integral transformation (hologram), the spectral density is localized in a narrow band in the form of focal spots corresponding to different numbers of interfering modes. The coordinates of the maxima of the focal spots are related to the radial velocity (velocity projection in the direction to the receiver) and the distance of the source through the spatial frequency scales of the interferogram variability. The interference spectral density on the interferogram accumulates incoherently and is distributed over the entire region of the hologram. Such a mechanism for distributing the spectral density of the noise emission of the source and interference provides high noise immunity of processing, significantly exceeding the noise immunity of known processing methods. The hologram records the amplitudes of the interfering modes and the phase difference between them in all intermediate states that the source successively passes during the observation time. The physical and mathematical principles of hologram formation were first described in [1,2].

When developing holographic processing [1−4], it was assumed that the oceanic environment is homogeneous, i.e. its characteristics in the space-time domain are unchanged. In many cases of practical interest, information is transmitted against the background of hydrodynamic perturbations that distort the interferogram and increase the number of intense focal spots in the hologram. A particular aspect of the stability of holographic processing with respect to regular perturbations of the waveguide depth and sound velocity in the water column was analyzed in [5].

In the presence of hydrodynamic perturbations, the interferogram can be approximately represented as the sum of source interferograms formed by an unperturbed (in the absence of a perturbation) and a perturbed waveguide. The 2D-FT transformation is a linear process, which allows the hologram to be considered as a linear superposition of the unperturbed and perturbed waveguide holograms. If the spectral densities of the unperturbed and perturbed holograms are separated, then the holographic processing is stable against hydrodynamic perturbations. In this case, the inverse transformation of the 2D-FT to the allowed spectral densities of the holograms will make it possible to observe the unperturbed and perturbed interferograms of the source field.

In inhomogeneous media, holographic interferometry was first used when

processing data from the SWARM-95 experiment [6–8], when intense internal waves (IIWs) on a stationary path (stationary source and receiver) led to horizontal refraction and interaction of acoustic field modes. It was shown that holographic processing resolves the interferograms of the unperturbed and perturbed fields [9,10]. Shortly thereafter, this effect was theoretically described and confirmed by the results of numerical simulation, and the errors in the reconstruction of unperturbed interferograms were estimated [11,12].

In this paper, we present and discuss the results of numerical simulation of holographic processing of noise emission from a moving source (with a fixed receiver) in the presence of IIWs, which determine the interaction of acoustic field modes. The effect of IIWs on the error in reconstructing the distance, the radial velocity of the source, and the interferogram of the unperturbed field is estimated.

2. CHARACTERISTICS OF INTENSE INTERNAL WAVES

Intense internal waves are a hydrodynamic phenomenon that is widespread in the oceanic environment. In shallow water areas, they represent trains of intense short-period fluctuations of the water surface of constant density, interpreted as trains of solitons that propagate towards the coastline at a speed of $u \sim 0.5$-1 and are separated by periods of calm $\delta L \sim 10$ km, which makes the pattern of the internal wave field non-stationary. The reason for their occurrence is due to internal tides: on the shelf, energy is transferred from internal tidal waves to short-period ones [13]. According to the experimental data, the length of the trains is $L \sim 2$-4 km, the period is $\Lambda \sim 200$-400 m (the distance between the crests of neighboring solitons), the half-width is $\eta \sim 50$-150 m, and the amplitude is $B \sim 10$-30 m [14-16]. Soliton trains are characterized by: a) anisotropy in the horizontal plane, the radius of curvature of the front is $r \sim 15$-25 km; b) quasi-sinusoidality in the direction of propagation, i.e. narrowness of the spatial spectrum; c) synchronism of vertical displacements in depth, which indicates the dominance of the first gravity mode. These properties determine the horizontal refraction and interaction of source field modes if the acoustic path is located at small and large angles to the soliton train wavefront, respectively [17,18].

3. NUMERICAL SIMULATION

To be able to compare the results of holographic processing for the cases of a stationary and moving source in the IIWs field, which determine the interaction of modes, the simulation data were chosen the same as in [12].

The depth distribution of the speed of sound is shown in **Fig. 1.** Two frequency

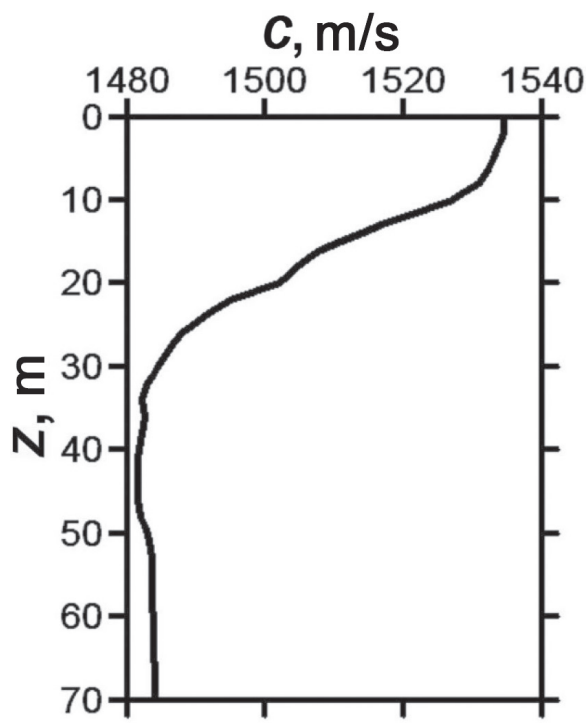

Fig. 1. *Unperturbed sound velocity profile* [8].

ranges were considered: Δf_1 = 100-120 Hz and Δf_2 = 300-320 Hz. Parameters of the liquid absorbing bottom: the ratio of the density of soil and water $\varrho = 1.8$; for the first frequency range Δf_1 the complex refractive index $n = 0.84(1 + i0.03)$, for the second frequency range Δf_2 – $n = 0.84(1 + i0.05)$. In the frequency range Δf_1 the field was formed by M = 4 modes, in the frequency range Δf_2 – M = 10 modes. Mode propagation constants $h_m(\omega_0)$ and their frequency derivatives $(dh_m(\omega_0))/d\omega$ at mid-range frequencies f_0 = 110.310 Hz are given in **Table 1, 2**. The scheme of the source movement relative to the IIW propagation is shown in **Fig. 2**.

At the initial time $t_0 = 0$, the distance between the moving source and the receiver is x_0 = 10 km. The source was located at a depth of z_s = 12.5 m, the receiver – at a depth of z_q = 35 m. The radial velocity of the source $w = -1$ m/s (when the source approaches the receiver, the radial velocity is negative, while moving away it is positive). A uniform spectrum was set. Pulses with duration $T = 4$ s (frequency sampling step 0.25 Hz) of sound pressure were recorded at intervals $T_* = 5$ s. The model of a single soliton was used. Soliton parameters: amplitude $B = 15$ m, half-width $\eta = 150$ m, velocity $u = 0.7$ m/s. The soliton moved in the direction from the source to the receiver, at the time $t_0 = 0$ it is removed from the receiver at a

Table 1

Frequency f_0 = 110 Hz.

Mode numbers, m	1	2	3	4
h_m, м$^{-1}$	0.4635	0.4557	0.4450	0.4310
$(dh_m/d\omega)/10^{-4}$, с/м	6.7624	6.8085	6.9014	7.0914

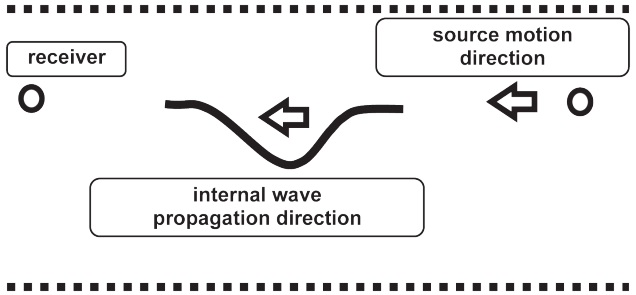

Fig. 2. *Scheme of source motion in the IIW field.*

distance x = 5 km. The observation time Δt = 20 min, during this time the soliton traveled the distance Δx = 840 *m*. The sound field at the receiving point was calculated within the modal approach of mode interaction.

The simulation results are shown in **Fig. 3-6**. The dotted line on the holograms shows the band in which the spectral density of the received signal is concentrated. Linear dimensions of the band: $\delta\tau \approx 0.15$ s, $\delta\nu \approx 0.002$ Hz, which is consistent with the theoretical estimates of the sizes of focal spots $\delta\tau = 0.1$ s, $\delta\nu = 0.0017$ Hz [1,2]. Here τ and ν are the time and frequency of the hologram.

Based on the first focal spot of the hologram closest to the origin, the radial velocity w and the initial distance x_0 are estimated as [1,2]

$$\dot{w} = -|k_w|\nu_1, \quad \dot{x}_0 = |k_x|\tau_1, \tag{1}$$

where

$$k_w = \frac{M-1}{h_{1M}(\omega_0)}, \quad k_x = \frac{M-1}{dh_{1M}(\omega_0)/d\omega}. \tag{2}$$

Here ν_1 and τ_1 are the coordinates of the maximum of the first focal spot; h_m is the real part of the horizontal wave number of the m-th mode, $h_{1M} = h_1 - h_M$. The restored source parameters, in contrast to the model values, are indicated by a dot at the top.

Table 2.

Frequency f_0 = 310 Hz.

Mode numbers, m	1	2	3	4	5	6	7	8	9	10
h_m, м$^{-1}$	1.3123	1.3073	1.3006	1.2920	1.2826	1.2730	1.2630	1.2525	1.2403	1.2258
$(dh_m/d\omega)/10^{-4}$, с/м	6.7511	6.7619	6.7813	6.7973	6.8080	6.8150	6.8312	6.8753	6.9703	7.0574

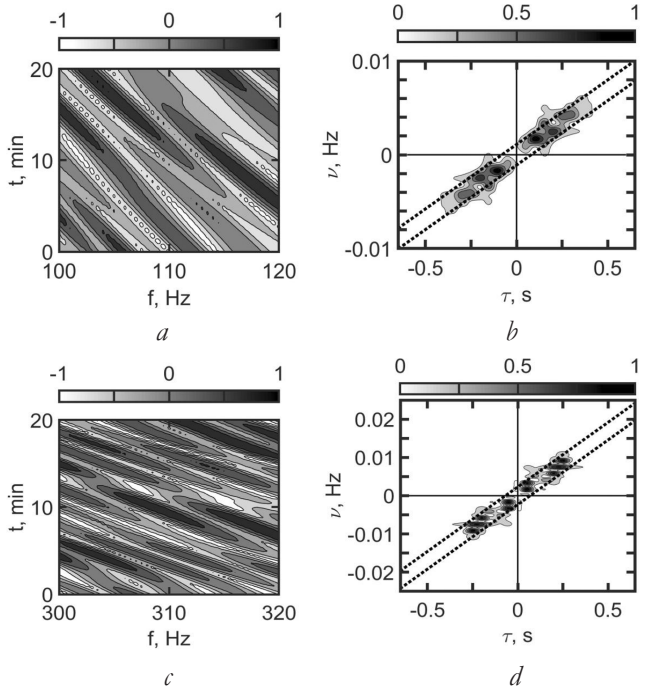

Fig. 3. *Normalized interferograms (a, c) and holograms (b, d) in the absence of disturbance: (a, b) – frequency range* Δf_1*, (b, d) – frequency range* Δf_2*.*

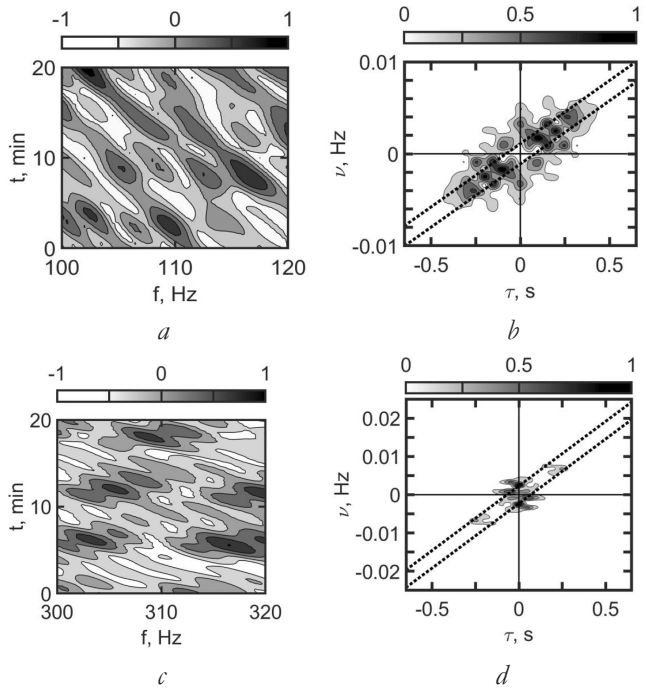

Fig. 4. *Normalized interferograms (a, c) and holograms (b, d) in the presence of a disturbance: (a, b) – frequency range* Δf_1*, (c, d) – frequency range* Δf_2*.*

On **Fig. 3** shows the interferograms and moduli of the source field holograms in the absence of perturbation. Interference fringe slopes: $\delta f/\delta t \approx -0.016$ s^{-2} (frequency range Δf_1) and $\delta f/\delta t \approx -0.035$ s^{-2} (frequency range Δf_2). Coordinates of the peak of the first focal spot: $\tau_1 = 0.1$ s, $\nu_1 = 1.71\cdot10^{-3}$ Hz (Δf_1); $\tau_1 = 3.80\cdot10^{-2}$ s, $\nu_1 = 0.002$ Hz (Δf_2). According to (1) and the data of Table 1, 2 restored source parameters: $\dot{w} = -0.99$ m/s, $\dot{x}_0 = 9.1$ km (Δf_1); $\dot{w} = -1.3$ m/s, $\dot{x}_0 = 11.1$ km (Δf_2).

The interferograms and moduli of the source field holograms as the soliton moves along the path are shown in **Figs. 4.** Perturbation of the aquatic environment leads to distortions of localized fringes of interferograms and the appearance of additional intense focal spots of holograms compared to the unperturbed medium. The spectral density along the localized fringes of interferograms becomes highly nonuniform, acquiring the form of focal spots (Fig. 4(*a,c*)). This mechanism becomes more acute with an increase in the frequency range, which is explained by an increase in the effect of scattering by inhomogeneities with increasing frequency. In the holograms (Fig. 4(*b,d*)) with an increase in the frequency range, the concentration of the spectral density along the frequency axis increases, which indicates the predominant influence of the perturbation on the formation of the hologram appearance.

The results of cleaning the spectral densities of the holograms from the perturbed field in the vicinity of the frequency axis ν and their Fourier image are shown in **Figs. 5**. The shape of the arrangement of spectral densities on the holograms of the unperturbed waveguide (Fig. 3(*b,d*)) and reconstructed in the presence of a perturbation (Fig. 5(*b,d*)) are close to each other. The peak coordinates of the first focal spot are estimated as: $\tau_1 = 1.19\cdot10^{-1}$ s, $\nu_1 = 0.002$ Hz (Δf_1); $\tau_1 = 4.08\cdot10^{-2}$ s, $\nu_1 = 1.63\cdot10^{-3}$ Hz (Δf_2). According to (1) and the data of Table 1, 2 restored source parameters

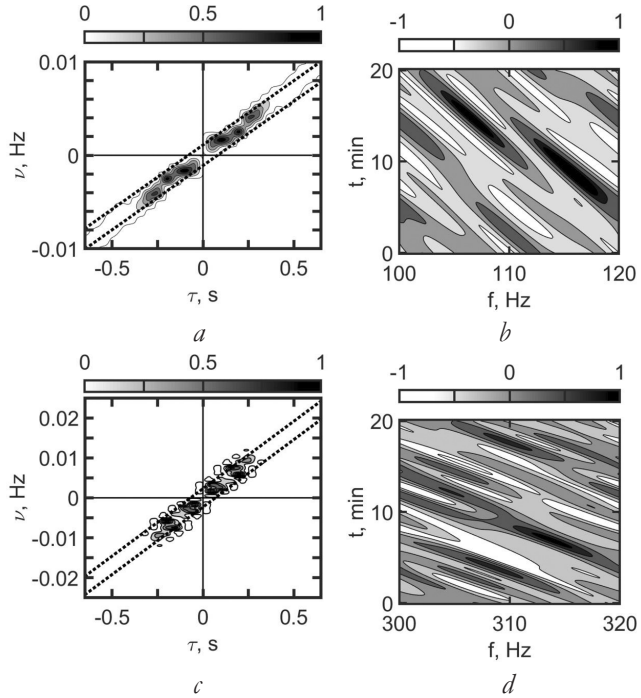

Fig. 5. *Normalized filtered modules of holograms (a, c) of the unperturbed field and interferograms reconstructed from them (b, d): (a, b) – frequency range* Δf_1*, (c, d) – frequency range* Δf_2*.*

$\dot{w} = -1.1$ m/s, $\dot{x}_0 = 10.8$ km (Δf_1); $\dot{w} = -1.1$ m/s, $\dot{x}_0 = 12.0$ km (Δf_2). The reconstructed interferograms of the unperturbed field in the presence of a disturbance are shown in Figs. 5(*b,d*). The slopes of the interference fringes are estimated as $\delta f/\delta t \approx -0.016$ s^{-2} (Δf_1) and $\delta f/\delta t \approx -0.035$ s^{-2} (Δf_2).

On **Fig. 6** shows one-dimensional normalized interferograms of unperturbed fields in the absence of a disturbance (solid line) and reconstructed (dots) in its presence. The normalized value is indicated at the top

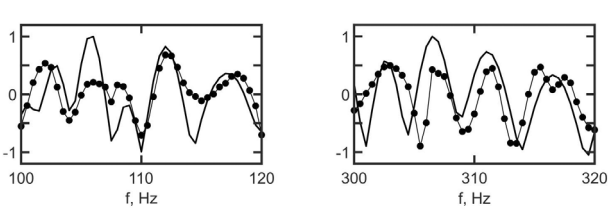

Fig. 6. *Dependences of normalized one-dimensional interferograms of unperturbed fields on frequency f in the absence of a disturbance (solid line) and reconstructed in its presence (dots): (a) frequency range* Δf_1*, (b) frequency range* Δf_2*.*

with the "lid" icon. The interferograms are horizontal sections of the corresponding two-dimensional interferograms (Fig. 3, 5). The error in the reconstruction of interferograms will be characterized by the quantity

$$d = \frac{\sum_{j=1}^{J} |I_1(f_j) - I_2(f_j)|}{\sum_{j=1}^{J} |I_1(f_j)|}, \qquad (3)$$

where the number of samples $J = 80$. Here $I_{1,2}$ is the interferogram of the unperturbed field in the absence of perturbation and reconstructed in its presence, respectively. For the frequency range Δf_1 Hz, the error is $d = 0.635$, for the frequency range Δf_2 Hz – $d = 0.821$. Compared to a stationary source [12], the error increased by a factor of 45.4 and 11.1 times for the frequency ranges Δf_1 and Δf_2, respectively. The indicated difference in the error values is explained by the different character of the medium variability. With a stationary source, there is a temporal variability of the oceanic environment, and with a moving source, there is a spatio-temporal variability. Thus, in the case of a moving source in the presence of IIW, the interferogram of the unperturbed field is not restored.

4. CONCLUSION

On the basis of numerical simulation data, the stability of the holographic method for detecting and localizing a moving underwater source against the background of IIWs, which determine the interaction of sound field modes, is considered.

In the case of a moving source, IIWs cause spatio-temporal variability of the aquatic environment, which leads to more significant distortions of the interferogram of the unperturbed field compared to a stationary source. In the presence of such strong distortions in the hologram, the

spectral density in the form of intense focal spots is concentrated mainly in the region of the frequency axis, which indicates the predominant effect of IIWs on the formation of the hologram. An essential factor in the formation of a hologram, as in the case of a stationary source, is the possibility of separating the spectral densities of the perturbed and unperturbed fields. This makes it possible to restore the hologram of the unperturbed field of a moving source with minimal distortions in the presence of IIWs and to estimate its parameters.

The results of the numerical experiment demonstrated the stability of the holographic method for detecting and localizing a moving underwater source against the IIWs sbackground. In the presence of IIWs and in their absence, the estimates of the radial velocity and remoteness of the source are close to each other. In contrast to a stationary source, in the case of a moving source, in the presence of IIWs, it is impossible to restore the interferogram of the unperturbed field. In this case, however, the angular coefficients of the interference fringes practically remain unchanged.

REFERENCES

1. Kuznetsov GN, Kuzkin VM, Pereselkov SA. Spectrogram and localization of a sound source in a shallow sea. *Acoustical Physics*, 2017, 63(4):449-461. DOI: 10.1134/S1063771017040078.
2. Kaznacheev IV, Kuznetsov GN, Kuzkin VM, Pereselkov SA. Interferometric method for detecting a moving sound source with a vector-scalar receiver. *Acoustical Physics*, 2018, 64(1):37-48. DOI: 10.1134/S1063771018010104.
3. Emmetiere R, Bonnel J, Gehant M, Cristol X, Chonavel Th. Understanding deep-water striation patterns and predicting the waveguide invariant as a distribution depending on range and depth. *J. Acoust. soc. Am.*, 2018, 143(6):3444-3454.
4. Emmetiere R, Bonnel J, Cristol X, Gehant M, Chonavel T. Passive source depth discrimination in deep-water. *IEEE J. of Selected Topics in Signal Processing,* 2019, 13(1):185-197.
5. Pereselkov SA, Kuz'kin VM. Interferometric processing of hydroacoustic signals for the purpose of source localization. *J. Acoust. soc. Am.,* 2022, 151(2):666-676.
6. Apel JR, Badiey M, Chiu C-S, Finette S, Headrick RH, Kemp J, Lynch JF, Newhall AE, Orr MH, Pasewark BH, Tielburger D, Turgut A, von der Heydt K, Wolf SN. An overview of the SWARM 1995 shallow-water internal wave acoustic scattering experiment. *IEEE J. Ocean. Eng.*, 1997, 22:465-500.
7. Frank SD, Badiey M, Lynch J, Siegmann WL. Analysis and modeling of broadband airgum data influenced by nonlinear internal waves. *J. Acoust. soc. Am.,* 2004, 116(6):3404-3422.
8. Badiey M, Katsnelson BG, Lynch JF, Pereselkov S, Siegmann WL. Measurement and modeling of three-dimensional sound intensity variations due to shallow-water internal waves. *J. Acoust. soc. Am.,* 2005, 117(2):613-625.
9. Kuz'kin VM, Pereselkov SA, Zvyagin VG, Malykhin AYu, Prosovetskiy DYu. Intense internal waves and their manifestation in interference patters of received signals on oceanic shelf. *Phys. wave phenom.,* 2018, 26(2):160-167.
10. Badiey M, Kuz'kin VM, Lyakhov GA, Pereselkov SA, Prosovetskiy DYu,

Tkachenko SA. Intense internal waves and their manifestation in the interference patterns of received signals on oceanic shelf. Part II. *Phys. wave phenom.*, 2019, 27(4):313-319.

11. Kaznacheeva ES, Kuz'kin VM, Pereselkov SA. Interferometric processing of hydroacoustic information in the presence of intense internal waves. *Phys. wave phenom.*, 2021, 29(3):278-284.
12. Kuzkin VM, Lyakhov GA, Pereselkov SA, Kaznacheeva ES. Transmission of information through a randomly inhomogeneous oceanic medium. *Fundam. appl. hydrof.*, 2021, 14(2):54-64.
13. Konyaev KV, Sabinin KD. *Waves inside the ocean.* St. Petersburg, Gidrometeoizdat Publ., 1992, 271 p.
14. Zhou J, Zhang XZ, Rogers PH. Resonant interaction of sound wave with internal solitons in the coastal zone. *Acoust. soc. Am.*, 1991, 90(4):2042-2054.
15. Silver AN. Manifestation of the properties of solitons in internal waves on the shelf. *Izv. Academy of Sciences of the USSR, Physics of the atmosphere and ocean*, 1993, 29(2):285-293.
16. Hsu MK, Liu AK, Liu C. An study of internal waves in the China seas and vellow sea using SAR. *Continental Shelf Res.*, 2000, 20(4-5):389-410.
17. Katsnelson BG, Pereselkov SA. Low-frequency horizontal acoustic refraction caused by internal wave solitons in a shallow sea. *Acoustical Physics,* 46(6):684-691. DOI: 10.1134/1.1326723.
18. Katsnelson BG, Pereselkov SA. Space-Frequency Dependence of the Horizontal Structure of a Sound Field in the Presence of Intense Internal Waves. *Acoustical Physics,* 50(2):169-176. DOI: 10.1134/1.1675872.